A pseudo-spectral simulation of the Cahn-Hilliard equation to describe the phase ordering dynamics of a multicomponent system

170153234
Department of Physics & Astronomy, University of Sheffield
(Dated: May 20, 2022)

The discovery of the ubiquity of biomolecular condensates within physiology has generated a great amount of interest and has resurrected the field of Liquid Liquid Phase Separation mechanics. This is due to the implications and possible innovations their study has for the medical, biological and material sciences. To contribute to these efforts several versions of a pseudo-spectral code have been developed, which are appropriate for modelling the long-term converging of multicomponent systems, which spontaneously phase separate due to a thermal quench. Owing to the implicit nature of treating the stiff terms, one can use larger time-steps than Explicit Euler methods, among other finite difference methods. The pseudo-spectral method can be easily extended to more components and greater spatial dimensions, and can model systems with order parameter dependent mobilities, as well as coarsening dynamics for both bulk and interfacial diffusion.

I. INTRODUCTION

The observations by Brangwynne *et al*[1] of the liquid droplet like behaviour displayed by P-granules, and the subsequent identification of other such structures[2][3][4][5] have demonstrated the ubiquity of biomolecular condensates within biology. This discovery has generated a significant amount of interest in the scientific community. In principle, a biomolecular condensate is a membraneless condensed liquid like droplet of macro-molecular components (*e.g.* proteins, nucleic acids etc.) suspended within a molecularly depleted or enriched phase[2]. (fig.1). Despite the lack of a membrane, these novel structures are thought to behave as biochemical reactors creating the ideal conditions for heightened biochemical reaction events, metabolic efficiency[6] and a maintained morphology for minutes to hours[7]. These constructs have been demonstrated to be necessary for important bodily functions including chromatin organisation, transcription and the immune response[8].

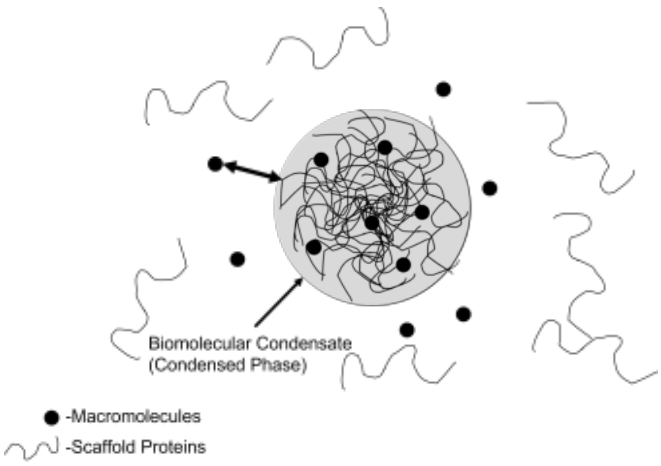

FIG. 1. A biomolecular condensate droplet (grey region) and its interactions with the molecularly depleted or enriched phase. The BC droplet is composed of various scaffold proteins, macro-molecules are freely exchanged between the dense and condensed phases.

The cell is somehow able to organise this discordant collection of macromolecules, numbering in the hundred or thousands into tens of co-existing phases of varying functional morphologies composed of specific biomolecular species. This intricate example of self-assembly is facilitated via Liquid-Liquid Phase Separation (LLPS), in which a liquid mixture composed of two or more substances de-mixes into two separate immiscible phases[9]. An intuitive example of LLPS is a vinaigrette salad dressing, the transient hydrophobic interactions of the non-polar oil and polar vinegar are sufficient to overcome unfavourable entropy associated with the more ordered de-mixed state. Therefore, the vinegar forms a sediment or suspension separate from the oil. Much of the enthusiasm towards biomolecular condensates, their formation and behaviour stems from the implication and applications their understanding has for medicine and the materials sciences. Aberrations in the processes which govern and generate biomolecular condensates are thought to contribute towards debilitating illnesses such as cancer and various neuro-degenerative diseases[10][8]. These aberrations are thought to be brought on by liquid solid phase separation, where droplet condensates increase in density forming fibrous, gel or solid-like aggregates, impeding the transport of macromoleules [11]. The exact mechanisms for how this occurs is till a mystery, however developing methods to describe how phase separated droplets develop their final packing structures could help bridge the gap towards this understanding[12]. Building on this, determining the parameters that dictate final droplet morphology is a desirable goal for the material sciences. Doing so may allows us to manipulate droplet formation, producing so called programmable droplets, possibly paving the way for developments in advanced adaptive and responsive materials and medical drug design.(Insert Citations Here).

From our exploration of the literature it appears that a significant amount of attention is focused upon IDP/R

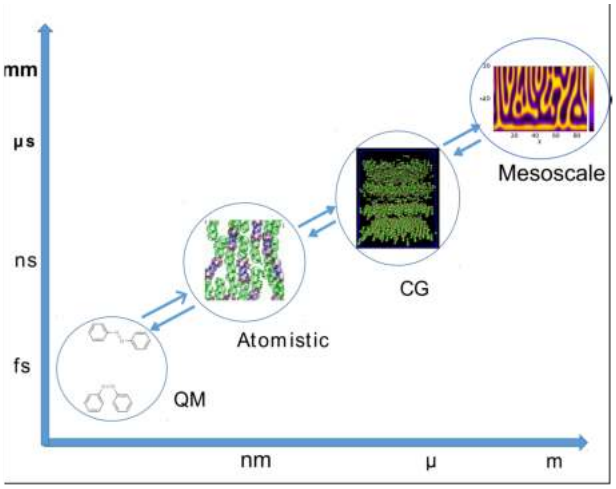

FIG. 2. A comparison of simulation scales for a varying abstraction. QM and Atomistic simulations are rich in detail, but are restricted to smaller length and time scales.

(Intrinsically Disordered Proteins/Region)[1]interactions, droplet rheology, biomolecular condensate and macromolecule identification and phase separation dynamics. Rheology and identification studies are usually conducted *in vitro* and *in vivo* via experimental analysis[14][15]. Phase separation dynamics are modelled with computational simulations at various length scales and complexities[16][17][18][19]. Experimental approaches have already been discussed at length in the literature review, as our project is focused on computational efforts they will be omitted. When attempting to simulate biological phase separation there are two factors that must be considered, the first is an appropriate model to approximate phase separation in the computational space. The second is the attention that must be place upon the scale and abstraction of the system, see *fig.*2 for a comparative illustration of these scales. As far as a model is concerned, Liquid Liquid Phase Separation has been studied extensively throughout the 20th century for synthetic polymers in solvents or polymer melts. A notable outcome of this work is the Flory Huggins general solution Theory[20] (see Section 1B), which has proven to be an accurate representation of regular polymer solutions after experimental analysis [21][22]. At its most rudimentary Flory Huggins Theory (FHT) is a representation of binary component systems, but has since been extended to multicomponent systems[23]. As such, FHT has seen application in some simulations exploring mesoscale LLPS dynamics in a biological context[24][25]. These endeavours have suggested that FHT free energy must be modified to include the effects of interfacial energy on droplet development which will be discussed later. Most other studies of multicomponet systems apply random matrix theory, pioneered by Frenkel and Jacobs[26][18]. This method only captures system outcomes at equilibrium rather than transience. The evolution of a chosen model must then be tracked using some form of dynamical simulation, this is where we must consider a simulation's architecture. Atomistic simulations have length scales of a few hundred nanometers and nanosecond timescales. They are useful for the study of intermolecular interactions between biopolymers and macromolecules, particularly the roles of different forces and molecule interactions within the nascent stages of phase separation. Atomistic simulations do have limits however, due to the handling of high resolution systems a significant amount of computation is required which reduces the simulations scope and observation time. A compromise is to reduce granularity with a coarse grained simulation; which treats groups of molecules of a system as pseudo-particles with averaged out effects tuned by the designer, in comparison to individual particle interactions. This is a more favourable approach for simulations of this scale, but is still limited for studying the evolution of coarsening and growth in biomolecular condensates. Timescales are limited to micro seconds. These previous examples serve their purpose well, but capturing the formation and evolution of biomolecular condensates requires a much larger time scales on the order of milliseconds and beyond. Therefore, we can turn to mesoscale simulations, where we treat molecular components holistically using a scalar density field. We can then perform molecular dynamics simulations applying numerical analysis or grid based Monte Carlo methods in order to approximate the bulk diffusion of material within the density field. Mesoscale simulations of this type are the favoured approach to studying the long term stability and evolution of multi component systems[18].

This paper hopes to be a proof of concept and to lay the groundwork for future research in this topic with our construction and demonstration of a general multicomponent psuedo-spectral simulation for LLPS. Taking a similar approach to Mao et al[24] we used the Cahn-Hilliard equation to capture system dynamics, and lessons from Pezzutti *et al*[27] guided our approach to the codes architecture. A psuedo-spectral scheme is suitable for our aims as it increases the ceiling on the time-step limit; thus simulations can run longer for a smaller penalty on computational power. This is desirable as certain phenomenon can only be observed after long time periods. We chose the Cahn-Hilliard equation (CHE), due to its conservation of the order parameter and the incorporation of interfacial parameters and long range transport dynamics which are both important for describing coarsening processes. Interfacial effects have been demonstrated in the literature and theory to have a noticeable impact on domain development[28][29], as droplet configuration is dictated by the minimisation of this energy.

[1] IDPs are proteins which are thought to be the main drivers of phase separation, and may possibly play a part in liquid to solid transitions. Their mercurial confirmations allow for a greater mutivalency, thus more favourable interactions with other macromolecules[13].

This factor has seen very little attention in our exploration of the literature, thus we also consider this factor in our simulations via the addition of extra terms in the free energy functional. We also wanted to understand how order parameter dependent mobility and interfacial stiffness parameters impacted droplet development. Due to the very little time afforded to this project, and the ambition of our scope, we were limited to only a superficial validation of our methods. From our analysis, the code appears to effectively and accurately describe coarsening and growth mechanics with very little error in order parameter conservation. As for the study of droplet development this topic can be left for others to build upon. To help facilitate these efforts we have provided appropriate methodology and analytical methods, the simulation code can be found via the github link in Appendix B.

II. METHODOLOGY

A. Flory Huggins and ϕ^4 Theory

We can describe the phase-ordering dynamics of a system which has undergone a quench into a state where conditions facilitate spontaneous phase separation with three stages. The first stage, Onset, sees the rapid formation of single phase domains or droplets, followed by growth where these droplets swell with the diffusion of surrounding material local to the droplet. With the depletion of the surrounding material growth slows, further aggregation occurs through the assimilation of smaller droplets into larger droplets by long range transport, a process called coarsening. We can describe onset and growth mechanics with an appropriate dynamical equation and a free energy equation possessing two minima representing the component phase densities of the systems relaxed state. Coarsening, however, is dependent on interfacial energy to determine how easily smaller droplets assimilate into larger ones. Therefore, the total free energy must include a bulk term $f_b(\phi)$ and a non-local gradient term $\kappa(\phi)(\nabla\phi)^2$ to account for energy costs associated with the spatial gradients of the density field. The κ coefficient embodies the interfacial stiffness of phase surfaces. Like mobility in a real system κ can be dependent on volume fraction, atomic interaction parameters and temperature[30]. In a regular solution κ is constant. Taking on these considerations, the general form of the free energy functional for d dimensions is thus:

$$\frac{\mathcal{F}[\phi(r,t)]}{k_B T} = \int \left[f_b(\phi) + \kappa(\phi)(\nabla\phi)^2 \right] d^d\vec{r} \qquad (1)$$

There are some generic features of the bulk free-energy, $f_b(\phi)$, irrespective of its functional form, which we discuss here. The shape of the bulk free-energy, $f_b(\phi)$ depends on temperature. At high temperatures, it is convex upwards and the mixed state with an uniform order parameter across the system is preferred (*fig.*)3a. However, as one lowers the temperature, $f_b(\phi)$, develops a non-convex region where $f_b''(\phi) < 0$, and this opens up a miscibility gap in the order parameter values and the system spontaneously phase separates in order to lower its free-energy (*fig.*)3b. This phase-separated state implies an order parameter which is positions dependent and as a result it costs surface energy penalty. Thus the final state of a phase separated system is one which tends to minimal area of the interface. The coarsening process is dictated by this type of free-energy functional.

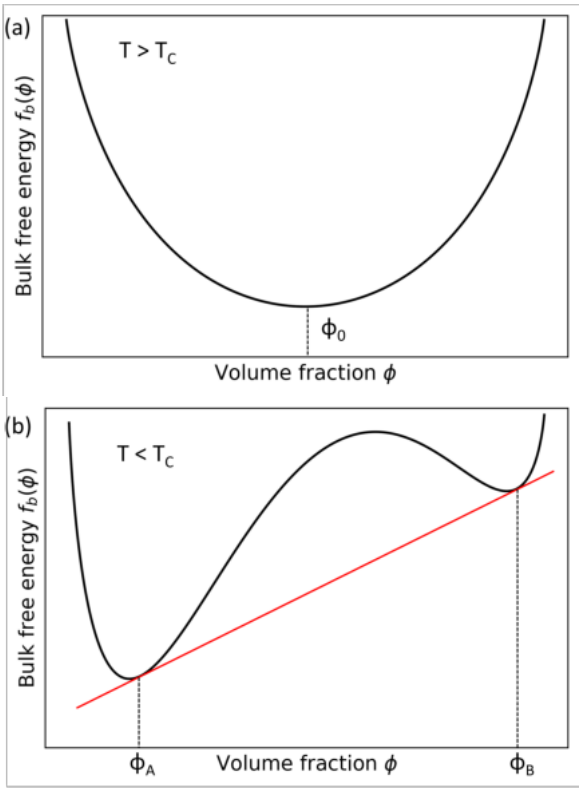

FIG. 3. Bulk free energies for asymmetric polymer mixed (a) and phase separated (b) system . ϕ_A, ϕ_B and ϕ_0 are the system's equilibrium compositions for a phase separated and mixed state.

Flory-Huggins general solution theory or FHT describes the phase behaviour or the thermodynamics of a mixed polymer solution and provides a desirable free energy expression. All system interactions and temperature are contained within a single variable, and the equation's simplicity allows the extension to multiple components. The general Flory-Huggins free energy equation for an incompressible binary polymer system can be described by the component polymer chain lengths N_A and N_B, temperature dependent interaction parameter χ and order parameter ϕ. Where ϕ in the context of soft matter physics is a system components volume fraction. For an n-component system a component's volume fraction ϕ_i is defined by its polymer chain length N_i and specific volume $\nu_i = \left(\frac{\partial V}{\partial n_i}\right)_{T,P,N_(j=1,2,3...N)}$ for the following ex-

pression[31]:

$$\phi_i = \frac{\nu_i N_i}{\sum_{j=1}^{N} \nu_j N_j} \tag{2}$$

The Flory-Huggins equation is thus:

$$\frac{f(\phi)_b}{k_B T} = \frac{\phi}{N_A} ln(\phi) + \frac{(1-\phi)}{N_B} ln(1-\phi) + \chi\phi(1-\phi) \tag{3}$$

The first two terms describe the systems entropic mixing energy, contributing to the systems favourability towards a mixed state and the third term is the enthalpic energy contribution, which favours phase separation. Where $\chi = A + \frac{B}{T}$ (A, and B are constants) is the temperature dependent miscibility parameter that determines whether a stable thermodynamic state is homogeneous (mixed) for $\chi < \chi_c$ or phase separated for $\chi > \chi_c$ where χ_c is a critical value specific to the system. The constants of the χ parameter are determined by the relative interactions between various species. Where T is the absolute temperature, and k_B the Boltzmann constant. As we are only considering a unimolecular mixture $N_A = N_B = 1$. After a mixed system undergoes a quench into a state where phase separation is more energetically favourable, the bulk mass of each component will diffuse to regions with lower chemical potential for that component. During this period the system is out of equilibrium and the component mass diffuses stochastically; slowing as the separated domains tend towards the coexistence volume fractions. At long time periods we consider the system to reach equilibrium where thermodynamic stability is maintained by the balance of the chemical and mechanical forces of each component *i.e.* $\mu_A = \frac{\partial F}{\partial \phi_A} = \mu_B = \frac{\partial F}{\partial \phi_B}$ (chemical potential) and $\Pi_A = \phi_A \frac{\partial F}{\partial \phi_A} - F = \Pi_B = \phi_B \frac{\partial F}{\partial \phi_B} - F$ (osmotic pressure *i.e.* pressure exerted by the bulk phases). We can demonstrate this proviso graphically in *fig.*3b. Here we draw a loci between the two minima ϕ_A and ϕ_B representing the coexistence volume fractions for the phase separated system. We call the loci joining the two minima the common tangent, as the gradients at the two coexistence densities are equal. For a series of free energy curves for varying values of χ we can determine the temperature-dependent coexistence densities, $\phi_A(T)$ and $\phi_B(T)$. The locus of the coexistence densities yields the binodal or the coexistence curve. Plotting the locus of the free energies inflection points (where $\frac{\partial^2 F}{\partial \phi^2} = 0$) gives us the spinodal line. The outcome of these tasks can be seen in *fig.*4, where the region within the spinodal is called the unstable region. The point of intersection between the spinodal and binodal is the critical point (where $\frac{\partial^3 F}{\partial \phi^3} = 0$) it is defined as the absolute minimum conditions (minimum ϕ and χ values) required for a system to phase separate. A system transitioning to the unstable region will undergo spontaneous phase separation, forming a labyrinthine de-mixed network, an example of this behaviour for a 50:50 binary mixture can be seen in *fig.*7. This process is called spinodal decomposition (SD). Another outcome occurs if the system transitions to the metastable region; the space enveloped by the binodal but adjacent to the spindoal in *fig.*4. In the metastable region as system can remain mixed until arbitrary energy fluctuations or impurities push the system to de-mix through nucleation(akin to how ice crystals are formed). The dominant component of the system (where $\phi_A > \phi_B$ or vice versa) remains the medium in which the lesser component is sequestered into concentrated droplets dispersed throughout the dominant component. After the initial quench to either the unstable or metastable region, the component domains formed by SD or nucleation go through coarsening and growth processes. This continues until an energetically favourable configuration is reached, where we can consider the system to be at equilibrium as while diffusion is still occurring it is not significant enough to cause changes to droplet sizes. The final morphology of droplets after growth and coarsening can vary randomly, binary systems evolve into a single droplet or sedimentary layers of opposite phases (zebra stripes). The morphology of ternary systems is still an open question in this field as there are many possible permutations for the organisation of these phases. Possible configurations are also governed by many other factors other than the random initial density distribution of components in the mixture but, predicting these outcomes will give us insight into how biology uses phase separation for creation of cell machinery and structures, among other things. The ternary structures identified by others include the core-shell (or Russian doll) structure and the Janus droplet, the latter is a mechanically stable composition of multiple interfacing droplets[24].

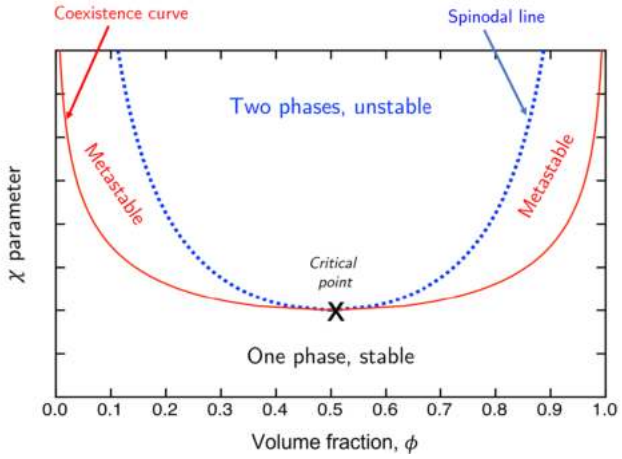

FIG. 4. A phase diagram for a binary system, displaying the binodal (coexistence curve), spinodal and critical point.

FHT's limitations do become apparent when studying intermolecular interactions in more detail, when accounting for hydrogen bonding, polymer self-interactions and the behaviour of salts, FHT's results do not agree with empirical data[32][33]. Although, FHT's flexibility allows

for the expansion of the χ parameter to model hydrogen bonding and other strong interactions as suggested by Wolf[33]. As we are not considering this level of detail FHT still serves our purposes, and this task can be left to those who wish to expand on this research.

While FHT is the most appropriate for modelling polymer mixtures, an analogous but simpler free energy expression is provided by scalar ϕ^4 theory a facet of quantum field theory, which has been previously applied to magnetic systems, solid solutions, lattice gas models *etc.*.Adapting the ϕ^4 potential energy equation to a system with temperature dependence we are given this expression for the bulk free energy[34]:

$$f_b(\phi) = \frac{-a}{2}(T_c - T)\phi^2 + \frac{b}{4}\phi^4 \tag{4}$$

Where a and b are constants, T is temperature and T_c is the systems critical temperature. Like with FHT, for $T > T_c$, the bulk free-energy has a single minimum, however, for $T < T_c$, the bulk free-energy exhibit two minima separated by a miscibility gap. Performing non-dimensionalisation ($\hat{\phi} = \frac{\phi}{\phi_0}$, where ϕ_0 is some constant) on the above expression for $T < T_c$ yields a free energy expression for a phase separated system, where the order parameter ϕ is confined to the range 1 and -1:

$$f(\phi) = \frac{\phi^4}{4} - \frac{\phi^2}{2} \tag{5}$$

The advantage of ϕ^4 over FHT free energy is the absence of the $ln\phi$ term leading to stabler simulations. Considering systems with $N_A = N_B = 1$ and assuming $T > T_c$, ϕ^4 theory proves to have a much more suitable replacement free energy for time intensive simulations.

B. Cahn-Hilliard Equation (Model B)

Mescoscale phase separation dynamics following a quench into the unstable or metastable region can be modelled using a number of non linear hydrodynamical stochastic PDEs. The standard naming scheme for these equations is alphabetical, they are models A-H. However, Berry *et al*[23] identifies models A, B, C and H as being sufficient for describing the growth and coarsening behaviour of phase separated systems. Because we do not need to explicitly consider hydrodynamic interactions as they are generally screened in polymeric liquids[35] we can eliminate model H. Model A is limited by its inability to describe long range mass transport and non-conserved order parameter, our concern is the evolution of phase behaviour for closed systems. Model B is the more suitable option due to its conservation of the order parameter and description of long range transport; required to describe coarsening. Model C is an amalgamation of both A and B and can also be discounted. Model B, or The Cahn-Hilliard equation can be generally expressed in the following way[36]:

$$\frac{\partial\phi(\vec{r},t)}{\partial t} = \nabla\cdot\left[M(\phi)\nabla\frac{\delta\mathcal{F}[\phi(\vec{r},t)]}{\delta\phi(\vec{r},t)} + \theta(\vec{r},t)\right] \tag{6}$$

The exterior divergence operator ensures the conservation of the order parameter and also a conserved noise and $M(\phi)$ is the mobility coefficient. The mobility coefficient determines the ease at which material is transported throughout the density field. For example the larger the volume fraction in some minute area the slower the rate of transport. This also applies to long polymer chains which are significantly slower than solvents for passive transport on account of polymer physical characteristics. The functional derivative term is the chemical potential field μ. To account for random thermal noise we include the stochastic noise term $\theta(\vec{r},t)$, which obeys the fluctuation-dissipation relation $\langle\theta_j(\mathbf{r},t)\theta_j(\mathbf{r}',t')\rangle = 2Mk_bT\delta_{ij}\delta(\mathbf{r}-\mathbf{r}')\delta(t-t')$; a relationship between the noise strength (left) and mobility. The inclusion of the noise term is necessary in simulations of nucleation and growth. The noise term mimics the random thermal noise which facilitate the formation and dissipation of droplets in the growth and coarsening phases of the process.As we are interested in studying the dynamics deep inside the spinodal regime, we do not include thermal noise in our simulations.

If we consider both κ and M to be constant the model B dynamical evolution equation is simplified further:

$$\frac{\partial\phi(\vec{r},t)}{\partial t} = M\left[\nabla^2\frac{\partial f_b}{\partial\phi} - 2\kappa\nabla^4\phi\right] \tag{7}$$

C. Solving the Cahn-Hilliard Equation

The Cahn-Hilliard equation does not poses an analytical solution, instead, its solution can obtained through some numerical integration method. A traditional approach would be to apply a discrete finite element numerical integration scheme, such as the explicit Euler method or Runge-Kutta. These techniques are hindered by the time step Δt limit of spatial discretization and the maximum time-step, $\Delta t_{max} \sim \Delta x^4$. As the spatial discretisation length, Δx, must be less than the interfacial width, z, the following inequality must be followed : $\Delta x < \sqrt{\kappa}$ (where $z\ \sqrt{\kappa}$, as the interfacial width scales as the square root of the order parameter stiffness, κ). However, the coarsening process is extremely sluggish, especially at long times, when typical domain sizes, $l(t)$ grows as $t^{1/3}$. This goes by the name of Lifshiz-Slyozov coarsening and thus the velocities of the front scales as $l(t)/t \sim t^{-\frac{2}{3}}$. Thus the coarsening rate becomes slower and slower during the late-stage coarsening. This renders the explicit Euler methods, with an upper limit of time-step, impractical [27]. Thus we have opted for a Spectral Numerical Integration Scheme to obtain the PDEs solution, more precisely the Fourier collocation method or

pseudospectral method, which is an unconditionally stable algorithm and allows for large time-steps. In contrast to the finite difference examples already stated, spectral methods are applied to an entire domain to produce an approximation for system evolution. What is meant by this? For a finite difference method one selects a local point within a domain and calculates its variance from neighbouring points. The psuedo-spectral method allows us to act globally across the domain as we transform the system to k-space. In doing this our PDE instead becomes a series of coupled differential equations for each point in k-space considered for the problem. The unique properties of the psuedo-spectral methods causes solution error to decrease rapidly towards 0 as the number of grid points $N \to \infty$. This quick convergence in error is a consequence of the Fourier Series' coefficients decaying rapidly in comparison the algebraic series of finite difference methods[37]. To implement the psuedo-spectral method, our first step is to represent our density function $\phi(r,t)$ as a sum of the product of some basis function $\psi_n(\vec{r})$ and the corresponding weighting factors $\hat{\phi}_n(t)$ for n reciprocal space lattice points.

$$\phi(r,t) = \sum_n \hat{\phi}_n(t)\psi_n(\vec{r}) \tag{8}$$

As we are considering our system in bulk, where the density fields follow periodic boundary conditions, we require a periodic trial function for $\psi_n(\vec{r})$. In this case we may use the trigonometric polynomial: $\psi_n(\vec{r}) = e^{i\vec{k}\cdot\vec{r}}$. Where $\vec{k} = \frac{2\pi n\vec{r}}{L}$ and L is the domain size. Again as we are dealing with periodic boundary conditions our domain n spans from $n = -N/2+1$ to $n = N/2$. Substituting this criterion into *eq.*8 yields an expression for the Fast Fourier Transform (FFT):

$$\phi(r,t) = \sum_{-N/2+1}^{N/2} \tilde{\phi}_n(t) e^{i\vec{k_n}\cdot\vec{r_j}} \tag{9}$$

Where ˜denotes a Fourier transformed variable. By multiplying both sides of the above equation by $e^{-i\vec{k}\cdot\vec{r}}$ and summing over our real space points *i.e.* $j = 0, 1, 2, 3..N$ we are left with the inverse FFT:

$$\tilde{\phi}_n(t) = \frac{1}{N}\sum_{j=0}^{N} \phi_n(r_j,t) e^{-i\vec{k_n}\cdot\vec{r_j}} \tag{10}$$

This above equation gives us a means to return our equation back from k-space to real space after we have calculated an approximation for the systems evolution. Substituting *eq.*9 into our most rudimentary variant of the Cahn-Hilliard equation *eq.*7 where both M and κ are constant, we are given a series of simpler coupled ODEs for each point in k-space. One can then apply a finite difference or other numerical integration method to determine a solution for these coupled equations in k-space. The solution in physical space is then obtained through an inverse FFT. In our case we, restructure our generalised psuedo-spectral Cahn-Hilliard equation into the Explicit-Euler scheme to derive an equation for time evolution of an old density field ϕ^n towards a new field ϕ^{n+1} [38]:

$$\tilde{\phi}^{n+1}(\vec{k}) = \tilde{\phi}^n(\vec{k}) - \Delta t\left[\mathbf{k}^2\left\{\frac{\partial f_b'}{\partial \phi'}\right\}_{\vec{k}}^n + \kappa\mathbf{k}^4\tilde{\phi}^n\right] \tag{11}$$

Where $\left\{\frac{\partial f_b'}{\partial \phi'}\right\}_{\vec{k}}^n$ is the Fourier transform of the expression $\frac{\partial f_b'}{\partial \phi'}$ and $\mathbf{k} = |\vec{k}|$. The free energy derivative term is non-linear in k-space and is responsible for the coupling of the different k modes. The fourth order term $\mathbf{k}^4\tilde{\phi}$ is linear, and therefore can be treated implicitly we can use this behaviour to again restructure our time evolution equation into a semi-implicit format[38]. In this case our linear fourth-order term is treated implicitly and non-linear terms are treated explicitly. We can thus write our time evolution equation like so:

$$(1 + \Delta t\kappa\mathbf{k}^4)\tilde{\phi}^{n+1}(\vec{k}) = \tilde{\phi}^n(\vec{k}) - \Delta t\mathbf{k}^2\left\{\frac{\partial f_b'}{\partial \phi'}\right\}_{\vec{k}}^n \tag{12}$$

Compounding all non-linear terms into a generic variable $N(\phi)$ and linear terms into the variable $L(\phi)$ produces the general format of the psuedo-spectral method as applied to more sophisticated variants of the CHE found in this paper:

$$\tilde{\phi}^{n+1}(\vec{k}) = \frac{\tilde{\phi}^n(\vec{k}) + \Delta t\tilde{N}_k(\phi^n)}{1 + \Delta t L_k} \tag{13}$$

All psuedo-spectral CHE simulations were conducted in python 3.8, the FFT and IFFT functions were taken from the scipy 1.8.0 library[39] and are based upon the Cooley and Tukey method[40]. The general structure of the python code can be found in *fig.*5. The gradient, Laplacian and biharmonic operations were all conducted using central difference theorem, 3-point stencil (5-point in 2D) and 5-point stencil (13-point in 2D) respectively. An example of 2D simulation output for a system undergoing spindoal decomposition can be found in *fig.*6, as expected we see the characteristic growth and coarsening processes for $t > 100$. $t = 1 - 100$ shows the spontaneous phase separation via spinodal decomposition, then proceeding onto coarsening from $t = 1 - 100$ with the thinning out of defects.

D. Considering κ and M with ϕ dependence

Our simulation of phase separation dynamics more closely approximates real systems with the inclusion of ϕ dependence for M and κ. We can adapt our general CHE where this is the case (see Appendix B for full derivation), with the addition and subtraction of a linear term to maintain the implicit explicit psuedo-spectral structure in *eq.*13. With this technique our non-linear and linear terms become:

$$N(\phi) = M(\phi)\nabla^2\mu(\phi) + \nabla M(\phi)\cdot\nabla\mu(\phi) + A\nabla^4\phi \tag{14}$$

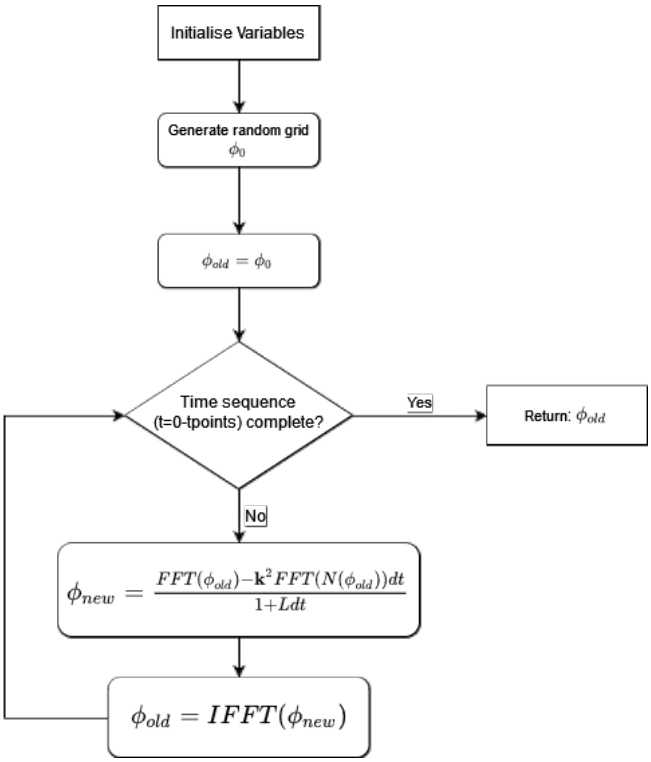

FIG. 5. Flowchart description of the python implementation for *eq.*13. Apart from the slight deviation in *eq.*12 for binary systems with constant mobility parameters, every other CHE simulation in this project is fundamentally based on this method

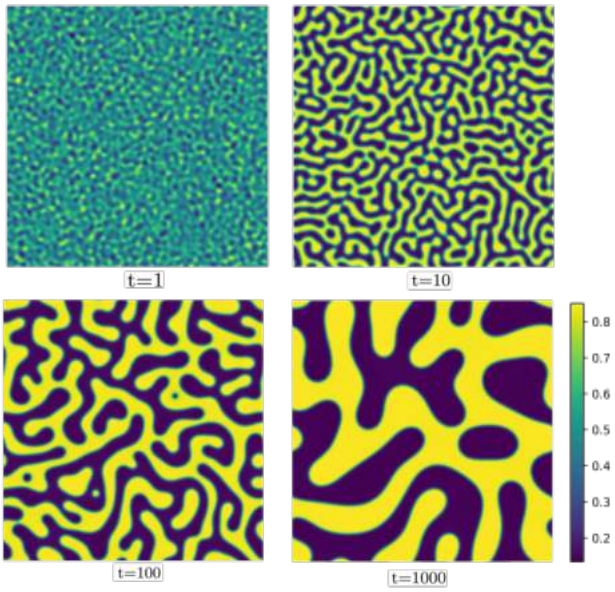

FIG. 6. Temporal snapshots of the direct output for an iteration of the Cahn-Hilliard equation with a Flory-Huggins free energy, for a binary 50:50 initial composition where $\chi = 2.5$ for constant mobility coefficients $D = 1$ and a constant order parameter stiffness, $\kappa = 1$. The simulation was performed for 1×10^5 time steps where $dx = 0.5$, and $dt = 0.5$, on a 512×512 grid.

$$L(\phi) = -A\nabla^4\phi \tag{15}$$

Where A is a stability constant to ensure mass drift is minimised. As the number of mathematical terms increases the simulation's stability decreases significantly, A is required to rectify this issue. Preliminary tests and the experiences of Pezzutti *et al*[27] suggests the optimal value is $A = \chi * \frac{1}{2}$, for ϕ^4 free energy this is a $\frac{1}{2}$. Due to limitations brought on by time and scope, we only considered non-constant M and treated κ as constant, however we have included an expression for both so others may build on this work. If we only treat κ as constant and express mobility as a function where $M(\phi = \frac{1}{2}) = 1$ and decreases as $\phi \to 0$ and $\phi \to 1$. This form of $M(\phi)$ ensures that the diffusion takes place at the interface ($\phi \sim 1/2$ for the Flory-Huggins free-energy and $\phi \sim 0$ for the ϕ^4 theory) and not in the bulk regions. The dynamics generated by interfacial diffusion is much slower than that arising from bulk diffusion and it can be quantified via the different exponents one observes in the growth law[27]. We can therefore express mobility like so:

$$M(\phi) = 1 - a(\phi + b)^2 \tag{16}$$

Where a is a constant controlling the rate at which mobility decreases and b is a graph transformation parameter. b allows this expression to be used for ϕ^4 where $b = 0$ and Flory-Huggins where $b = -\frac{1}{2}$. Considering only non-constant mobility are non linear and linear terms are thus:

$$\begin{aligned} N(\phi) = (1 - a(b+\phi)^2)\nabla^2\mu(\phi) \\ - 2a(b+\phi)\nabla\phi \cdot \nabla\mu(\phi) + A\kappa\nabla^4\phi \end{aligned} \tag{17}$$

$$L(\phi) = -A\kappa\nabla^4\phi \tag{18}$$

E. Ternary Systems

Mao *et al*[24] have already demonstrated a working multicomponent psuedo-spectral numerical integration scheme, thus we will adapt their methods for our ternary system simulation. Using their approach, the Flory-Huggins free energy equation can be extended to an incompressible N-component system with the addition of extra component specific χ parameters and gradient terms:

$$\frac{f_b(\phi)}{k_B T} = \left[\sum_{i=1}^{N} \phi_i ln\phi_i + \frac{1}{2} \sum_{i,j=1}^{N} \chi_{ij}\phi_i\phi_j + \frac{\kappa}{2} \sum_{i,j=1}^{N} \chi_{ij}\nabla\phi_i\nabla\phi_j \right] \tag{19}$$

Where $\chi_{ii} = 0$, $\chi_{ij} = \chi_{ji}$, κ is the stiffness coefficient, T is the absolute temperature and k_B is the Boltzmann

constant. Applying the same process of functional minimisation and non-dimensionalisation for the multicomponent free energy equation produce the N-component chemical potential μ:

$$\mu_i = 1 + ln\phi_i + \sum_{j=1}^{N} \chi_i j(1 + \kappa\nabla^2)\phi_j \tag{20}$$

As with our previous derivations, we can substitute the μ_is and ϕ_is into our multicomponent Cahn-Hilliard equation, neglecting the noise term $\theta(\vec{r}, t)$:

$$\frac{\partial \phi_i}{\partial t} = M\nabla \cdot \left[\phi_i \sum_j (\delta_{ij} - \phi_j)\nabla\mu_j \right] \tag{21}$$

For this investigation's ternary simulation we chose to treat M and κ as constants, although it is possible to apply the same methods in the previous section to more accurately replicate real world phase separation. We leave this task for others to build upon. It is also assumed that the $M_1 = M_2 = M_3$. As we assume incompressability *i.e.* $1 = \phi_1 + \phi_2 + \phi_3$ we are only required to track the phase behaviour of two components. Therefore our non-linear $N_i(\phi_i)$ and linear $L_i(\phi_i)$ components for the pusedospectral scheme take these forms:

$$N_i(\phi_i) = D\nabla \cdot \left[\phi_i \sum_j (\delta_{ij} - \phi_j)\nabla\mu_j \right] + AD\kappa\nabla^4\phi_i \tag{22}$$

$$L_i(\phi_i) = -AD\kappa\nabla^4\phi_i \tag{23}$$

III. COMPUTER SIMULATION RESULTS

All python simulations were conducted on the University of Sheffield's high performance computing architecture SHARC, using 16GB of RAM. The simulation space was a 1D grid of size $N = 512$, uniform distance between grid points $\Delta x = 0.5$ and length $L = N\Delta x = 256$. Periodic boundary conditions were in effect. The binary and ternary simulations with constant $D = 1$ and $\kappa = 1$ both had a time step of $\Delta t = 1$. The binary simulation used the Flory-Huggins free energy function. The interaction parameters for the ternary simulation were $\chi_{13} = \chi_{12} = 2.7$ and $\chi = 5$. The binary simulation with non constant $D = 1 - a(\phi + b)^2$ and $\kappa = 1$ had a time step of $\Delta t = 0.05$, due to non-negligible mass drift. Results for the binary phase diagram in *fig.*7 were obtained from the average of three runs with different random initial states ϕ_0, each of length 10^5 time steps, for increasing values of χ (range 2.05-2.65, step-size=0.05). Again $D = \kappa = 1$ and the same three initial fields were used for each χ value. Simulation snapshots in *fig.*6 and *fig.*9 were obtained for particular time steps increasing by log_{10} due to the large time period required to observe coarsening and growth. All random initial fields were generated using the 'random.uniform' function in the numpy 1.22.3 library[41]. For the ϕ^4 free energy function, numbers were generated in the range -1-1 and scaled by 0.05, for the FHT function this range was 0-1 and was not scaled. For the ternary simulation initial fields were generated from a homogeneous field equal to the components initial composition plus some bias field created using the same method applied to ϕ^4 field generation.

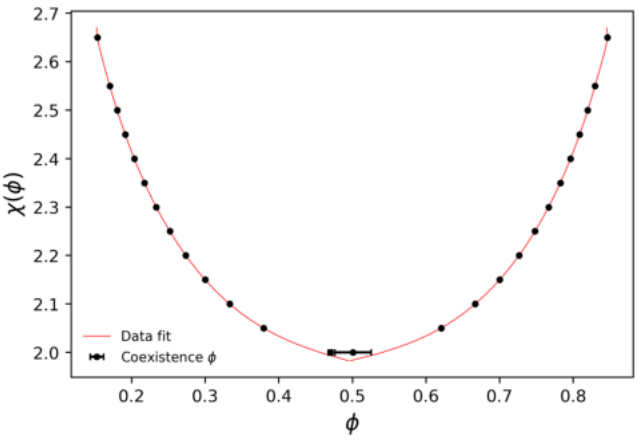

FIG. 7. The binodal for the average coexistence ϕ values obtained from the CHE simulation using Flory-Huggins free energy for a 50:50 mixture. Standard errors for ϕ are present. Model fit was calculated from a 20th degree least squares polynomial fit.

A. Method Validation

To ensure the characteristics of the Flory-Huggins free energy equation were conserved throughout the simulation, and in turn demonstrate its accuracy, we estimated the binodal line once the simulation reached equilibrium, the results can be found in *fig.*7. Through repeated observations, simulation activity decreased significantly after $t = 10^5$ for any time-step, we assume equilibrium at this point as coarsening is negligible. The binodal's coexistence values were calculated from a histogram of the final $\phi(\vec{r}, t)$ field, taking the average of the range for the largest bin. A 20th degree least squares polynomial fit was used to approximate the coexistence curve. There seems to be only minute variance in coexistence values for $\chi > \chi_c$, as $\chi \to \chi_c$ error increases significantly. This anomaly is to be expected however, as it is well documented that quenches near the critical point exhibit more complex dynamics [42]; our simulation is likely to be too simplistic to capture this behaviour. For quenches just above χ_c our CHE simulation seems to model a binary phase system appropriately which agrees with the theory. The simulation's strength is further reinforced by the 2D output for a quench towards the unstable (*fig.*6)

and metastable regions, where the system exhibited spinodal decomposition as well as growth and coarsening for the unstable quench. These results conform with work done by others[43]. In the metastable simulation we observed the expected nucleation events, although these did not further develop via coarsening due the lack of thermal noise.

To ensure appropriate behaviour when accounting for order parameter dependent mobility we also took samples from when the simulation enters the coarsening regime and compared them to circumstance where $M = 1$, these results can be found in *fig.*8. Although domain growth rate is exceptionally slow in this stage we can observe larger and fewer domains for the case where mobility is constant. For $t = 10000$ the $M(\phi)$ graph begins to exhibit these large domains as interracial transport continues. If we increase the a parameter, we would expect mobility to decrease further in regions of higher densities as described in *eq.*16. If this is the case we would observe a higher deviation in domain development between the two conditions in *fig.*8. We will go on to describe how to quantitatively describe these growth rates in section 3b.

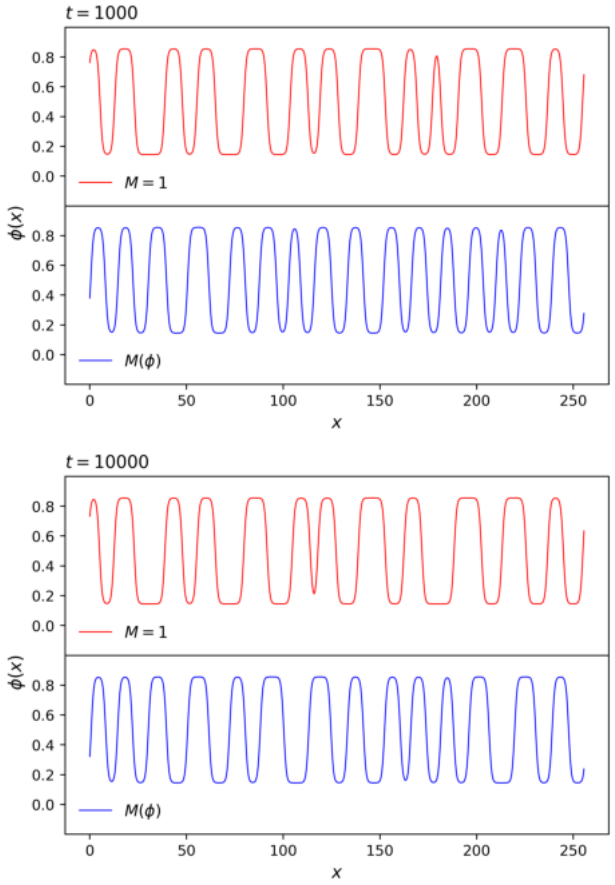

FIG. 8. A comparison of density fields $\phi(x)$ for binary simulations with $M = 1$ and $M(\phi)$. Where $M(\phi)$ coefficient $a = \frac{1}{3}$. In this iteration FH free energy was used for $\chi = 2.5$.

To verify the equilibrium condition of chemical potential μ balance, for coexisting ϕ values still held for systems where the number of components $n > 2$, we recorded μ for each component. An example plot of μ evolution for a single component can be found in *fig.*9 and a plot of all three component μs and $\phi(x, t)$ fields can be found in *fig.*10. Depending on the chosen confirmation of χ_{12}, χ_{13} and χ_{23} and initial volume fractions , we find a metastable 2-phase coexistence for $\mu_A = \frac{\partial F}{\partial \phi_A} = \mu_B = \frac{\partial F}{\partial \phi_B}$ where $\chi_{lk} >> \chi_{ij}, \chi_{ij}$ (l and k are components that repel each other strongly) or 3-phase coexistence for $\mu_A = \frac{\partial F}{\partial \phi_A} = \mu_B = \frac{\partial F}{\partial \phi_B} = \mu_C = \frac{\partial F}{\partial \phi_C}$ where $\chi_{12} = \chi_{13} = \chi_{23}$.

The evolution of μ for ϕ_A in *fig.*9 allows us to qualitatively describe the systems development as it passes through each regime, from $t = 0 - 10$ μ collapses from a random distribution to slight variance around a single value. Following this, at $t = 1000$ growth takes place as heterogenous regions accumulate material, resulting in minima and maxima. In the minima domains of ϕ_A begin to grow via bulk diffusion as material from the maxima is repelled by the other component domains. For $t > 1000$ interfacial diffusion is dominant as smaller droplets shrink and are consumed by larger droplets, we see this in the figure from the flattening out of some parts of the potential. After $t > 10^5$ large potential wells form, these will gradually widen as coarsening continues, at this point interfacial diffusion is minute and we can assume that the system has reached an equilibrium. *fig.*9b shows the output for a ternary simulation where $\chi_{12} = 2.7$, $\chi_{13} = 2.7$ and $\chi_{23} = 5$ after long time period $t = 10^6$. As expected we see characteristic maxima and minima for regions of a dominant phase, in this case the system has separated into two stable phases dominated by ϕ_B and ϕ_C (denoted by the balanced chemical potentials in *fig.*9a), and a metastable phase dominated by ϕ_A. In a real system this should not be the case, and instead we should observe three stable phases for each component. Of course, the reason for this error is due to the failure to include thermal noise, as indicated by the chemical potential plot there are regions of relative stability in which a metastable droplet can form. This metastable droplet only collapses if the system has significant energy to jilt the components from this potential well. If we stick with conditions where the quench is into the spinodal region for a multicomponent system *i.e.* where $\chi_{12} = \chi_{13} = \chi_{23}$, then this model more closely approximates real phase behaviour.

To ensure order parameter conservation the psuedo-spectral schemes' mass drift was also recorded, results for the binary simulation can be found in *fig.*11 and in *fig.*12 for the ternary system. For our binary simulations time step size is significantly larger than the limit imposed by $\Delta t >> \Delta x^4$, this ceiling can be pushed further for ϕ^4 simulations to around 5, after this value stability decreases rapidly. For binary simulations with non-constant M time step must be reduced by a factor of 100 to ensure stability, it is possible that this is a consequence of additional nonlinear terms. In the case of the ternary

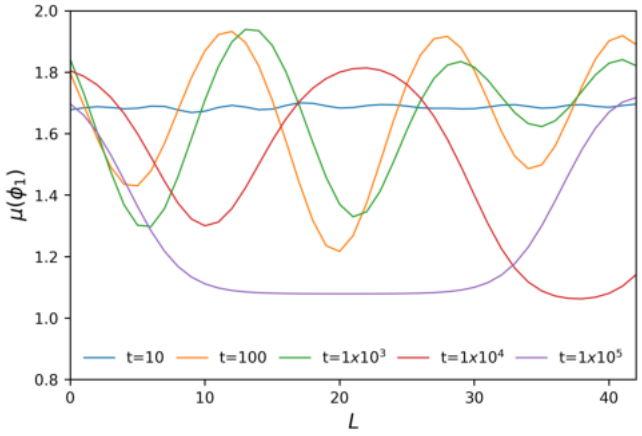

FIG. 9. The extract from a 1D grid of $L = 256$ for the evolution of chemical potential $\mu(\phi_A)$ for a ternary system, taken from a series of simulation snapshots.

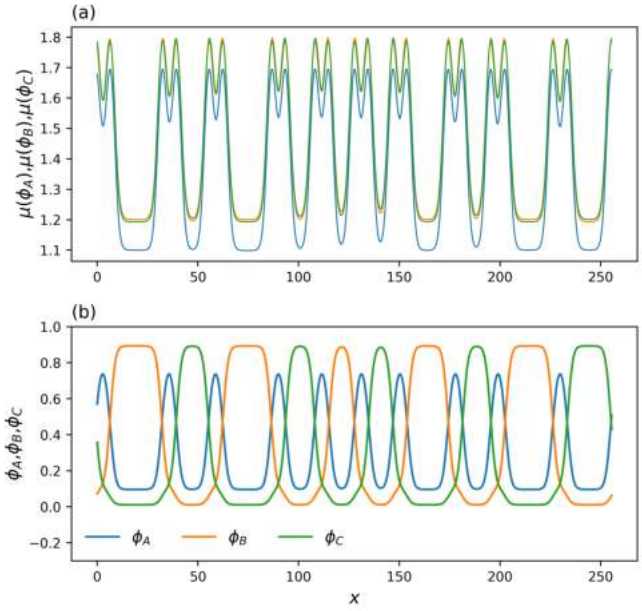

FIG. 10. The extract from a 1D grid of $L = 256$ at $t = 10^6$ for the evolution of chemical potential $\mu(\phi)$ and density field $\phi(x,t)$ for each component of a ternary system. Where $\chi_{12} = 2.7$, $\chi_{13} = 2.7$ and $\chi_{23} = 5$ and initial compositions $\phi_A = 0.3$, $\phi_B = 0.4$ and $\phi_B = 0.3$.

system, time step size can reach an order of magnitude higher than that of the binary system and still maintain mass conservation, unless χ values are large which results in spontaneous instability for $\Delta t = 10$. This is a quite bizarre outcome, although pseudo-spectral stability does increase for larger grid sizes this was not the case for a 2D lattice in our binary simulation runs, where step size was still limited to around 5. We don't have an answer to why this occurs, but it could be a mistake in the code itself as the methodology used in the binary and ternary

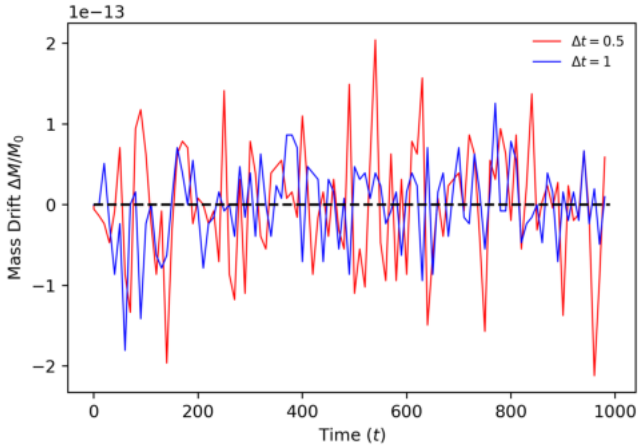

FIG. 11. The mass drift for a binary CHE simulation. Negligible drift is shown for $\Delta t >> \Delta x^4$.

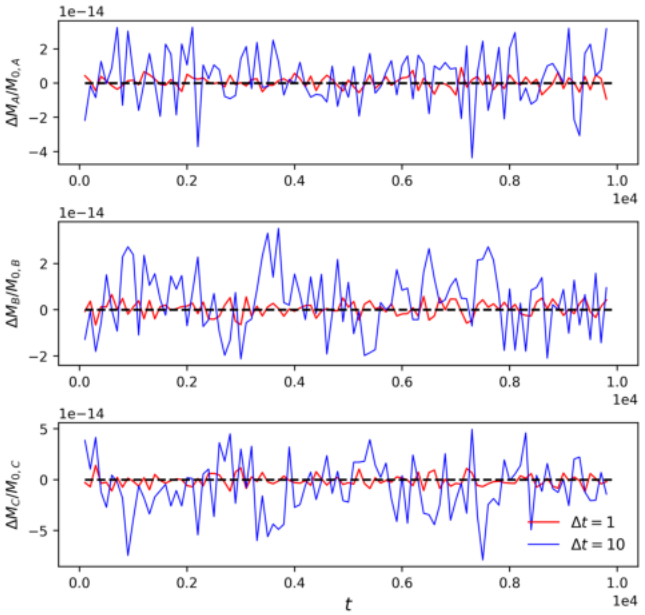

FIG. 12. The mass drift for each density field of a Ternary CHE simulation. Negligible drift is shown for $\Delta t >> \Delta x^4$.

simulations are slightly different (see Section 2B). It may be useful to rewrite the binary code in the ternary format and assess this issue. It is also pertinent to test whether the inclusion of a non-constant mobility term in the ternary code results in the same stability issues as the binary code.

B. Droplet morphology and phase development

Once a system quenches into the spinodal region compositional irregularities (regions abundant with one component) rapidly grow into domains with a characteristic

length L. Once the system enters the coarsening regime these domains will grow according to some exponent law $L(t) \approx t^{\alpha}$[44], in order to verify the accuracy of our simulation it is important to verify whether this exponent law converges towards the growth rate $\alpha = \frac{1}{3}$, as identified in the literature[42][45]. For cases where mobility depends on the order parameter, coarsening slows significantly, in this case previous work has identified the growth law to be dependent on $\alpha = 1 + a$ (a being the coefficient from *eq.*16)[45], this too should be confirmed. It has also been demonstrated that $\alpha = \frac{1}{3}$ holds for multicomponent systems with static mobility, this is even the case for nested morphologies, although the individual components of these structures violate this law[24], the composite droplet coarsening converges on $\alpha = \frac{1}{3}$. As we did not have time to run this calculation, we will instead state the methodology for others to complete. The characteristic length can be related to the time dependent structure factor $S(\vec{k}, t)$, which is dependent on the Fourier transformation of $\phi(\vec{r}, t)$ for each grid point in the lattice so that the wave vector $\vec{k}$ takes the discrete values $\frac{2n\pi}{N\Delta x}$ where n_x and n_y lie in the range $-N/2$ to $1-(N/2)$. The structure factor is therefore defined as[45]:

$$S(\vec{k}, t) = \langle \phi(\vec{r}, t)\phi(\vec{r}, t)^* \rangle \tag{24}$$

The structural factor is then related to the characteristic length in the relationship below:

$$L(t) = \frac{\int \vec{k} S(\vec{k}, t) d^3\vec{k}}{\int \vec{k}|\vec{k}| S(\vec{k}, t) d^3} \tag{25}$$

Plotting *eq.*25 for the simulation's run time allows us to approximate the exponent growth law and determine the parameter α.

As described by Mao et al, unique droplet packing morphologies arise from the need to minimise interfacial energy across the system, labelling interfacial surface tension between phase with the parameter σ_{ij}. To clarify this point, we can provide an example of a three-phase system ($sigma_{AB} > \sigma AC > \sigma BC$) with two possible outcomes, mechanically stable (top) or unstable state (bottom):

$$\sigma_{AB} < \sigma_{AC} + \sigma_{BC} \tag{26}$$

$$\sigma_{AB} > \sigma_{AC} + \sigma_{BC} \tag{27}$$

In the stable example components A, B and C do not wet each other, quantitatively described by a finite contact angle between phase interfaces. These conditions lead to the formation of Janus droplets, which are described as a cluster of multiple phases. For the unstable example one phase wets the other two which can lead to the core shell microstructure. Assessing these claims require us to obtain surface tensions from simulation output for a system at equilibrium we can integrate the density field between two phase coexistence fractions ϕ_1, ϕ_2[46]:

$$\sigma = \kappa \int_{\phi_1}^{\phi_2} \frac{dn}{dz} dn \tag{28}$$

These calculated σ values can then be compared with the interfacial inequalities to determine phase wetting behaviour.

C. Limitations of this approach

We have extensively discussed why failing to account for thermal noise prevents this system from fully replicating dynamic behavior outside of the spinodal, it is crucial to include metastable dynamics when studying multicomponent systems as these systems can contain both metastable and unstable phases as we saw in *fig.10*. However, we should also contemplate other improvements to the methodology. To start, Mao *et al* state that there foray into droplet microstructure was limited due to the restrictions imposed by the Flory-Huggins model's lack of free parameters to describe many phases, which limits the number of surface tension inequalities used to describe the mechanical state of droplets. Due to this there may be many arbitrary droplet configurations not yet observed. The extensive work on wetting dynamics by Koga and Widom may provide a suitable alternative to FHT in this regard, they have already succeeded in deriving density functional models for infinite order transitions in systems of two and three components[47][48].

As our project stands, it is more suitable for exploring synthetic unimolecular and polymer systems, this is still desirable as this work may help with the development of programmable droplets for the materials sciences. However, researching biological systems will require a more sophisticated free energy with the inclusion of extra terms to describe more complex intermolecular interactions such as hydrogen bonding as described by Wolf[**Wolf2020**]. Biomolecular condensate genesis within the cell involve may biochemical reactions as components are broken down and reformed, Shrinivas and Brenner include a term to account for these interactions in their dynamical equation which changes the flux of a component depending on a constant k[25]. They discovered that an increase in biomolecular turnover rate results in a decreased number of coexisting phases, a possible explanation as to why cells are not saturated with separate phase structures.

IV. DISCUSSION

In this paper we designed, constructed and assessed a pseudo-spectral python code which can be applied to binary and multicomponent systems in order to study phase development via growth and coarsening processes. We also demonstrated how surface tension measurements obtained from the simulation can be used to describe the characteristics of certain droplet microstructures. Performing these assessments for varying interfacial and interaction parameters may provide the knowledge to fine tune synthetic droplet structure development; a boon for

pharmaceutical and materials sciences.

The code's pseudo-spectral architecture allows for significantly larger time increments in comparison the explicit finite difference schemes. The intended flexibility of our work allows one to simulate conditions in which mobility and interfacial stiffness is related to the order parameter, to provide a more realistic model. This inclusion will allow for the exploration of order parameter dependent interfacial stiffness on droplet morphology, something not yet touched upon in the literature to our knowledge. Although we were not able to explore the codes full capabilities, we were able to verify its integrity by demonstrating its accurate replication of phase behaviour for binary and ternary systems. To make up for this lack of results We have provided guidance and direction for those who wish to continue this work. Limited time prevented us from verifying the coarsening growth laws observed in the literature, therefore care should be taken to ensure this has been confirmed before results can be obtained. The omission of thermal noise in our simulations means that coarsening behaviour of metastable phases cannot be described accurately, but quenches into the unstable region produce expected results and conform to mathematical predictions of phase coexistence and chemical potential balance. Finally, we have also suggested improvements to our methodology with the inclusion of a more sophisticated free energy to describe wetting mechanics for systems containing many phases transitions, and the inclusion of terms to describe component turnover from biochemical reactions inside the cell.

ACKNOWLEDGEMENTS

I would like to thank Biswaroop Mukherjee for his extremely helpful guidance on the practical part of this project, and assistance in helping me understand the complicated theory behind this topic. This dissertation wouldn't be finished to this standard if it wasn't for his help. I thank my supervisor Buddhapriya Chakrabarti for his support while I wrote the literature review, and throughout the project. I thank Diane Newton for the grammar and spell check. And Finally, I thank those friends and family members who have been there for me throughout this difficult year.

REFERENCES

[1]C. P. Brangwynne, C. R. Eckmann, D. S. Courson, A. Rybarska, C. Hoege, J. Gharakhani, F. Jülicher, and A. A. Hyman, "Germline p granules are liquid droplets that localize by controlled dissolution/condensation", Science **324**, 1729–1732 (2009).

[2]S. F. Banani, H. O. Lee, A. A. Hyman, and M. K. Rosen, *Biomolecular condensates: organizers of cellular biochemistry*, May 2017.

[3]J. A. Riback, C. D. Katanski, J. L. Kear-Scott, E. V. Pilipenko, A. E. Rojek, T. R. Sosnick, and D. A. Drummond, "Stress-triggered phase separation is an adaptive, evolutionarily tuned response", Cell **168**, 1028–1040.e19 (2017).

[4]C. P. Brangwynne, T. J. Mitchison, and A. A. Hyman, "Active liquid-like behavior of nucleoli determines their size and shape in xenopus laevis oocytes", Proceedings of the National Academy of Sciences of the United States of America **108**, 4334–4339 (2011).

[5]X. Chen, X. Wu, H. Wu, and M. Zhang, *Phase separation at the synapse*, Mar. 2020.

[6]Z. Gao, W. Zhang, R. Chang, S. Zhang, G. Yang, and G. Zhao, "Liquid-liquid phase separation: unraveling the enigma of biomolecular condensates in microbial cells", Frontiers in Microbiology **12**, 2866 (2021).

[7]Y. Shin and C. P. Brangwynne, *Liquid phase condensation in cell physiology and disease*, Sept. 2017.

[8]B. Wang, L. Zhang, T. Dai, Z. Qin, H. Lu, L. Zhang, and F. Zhou, *Liquid–liquid phase separation in human health and diseases*, Dec. 2021.

[9]R. A. L. Jones, *Soft condensed matter* (Oxford University Press, 2002).

[10]S. Alberti and A. A. Hyman, "Are aberrant phase transitions a driver of cellular aging?", BioEssays **38**, 959–968 (2016).

[11]A. L. Darling and J. Shorter, *Combating deleterious phase transitions in neurodegenerative disease*, Apr. 2021.

[12]S. Elbaum-Garfinkle, "Matter over mind: liquid phase separation and neurodegeneration", Journal of Biological Chemistry **294**, 7160–7168 (2019).

[13]P. Kulkarni and V. N. Uversky, *Intrinsically disordered proteins in chronic diseases*, Apr. 2019.

[14]D. M. Mitrea, B. Chandra, M. C. Ferrolino, E. B. Gibbs, M. Tolbert, M. R. White, and R. W. Kriwacki, *Methods for physical characterization of phase-separated bodies and membrane-less organelles*, Nov. 2018.

[15]M. Linsenmeier, M. R. Kopp, S. Stavrakis, A. de Mello, and P. Arosio, "Analysis of biomolecular condensates and protein phase separation with microfluidic technology", Biochimica et Biophysica Acta (BBA) - Molecular Cell Research **1868**, 118823 (2021).

[16]J. A. Joseph, A. Reinhardt, A. Aguirre, P. Y. Chew, K. O. Russell, J. R. Espinosa, A. Garaizar, and R. Collepardo-Guevara, "Physics-driven coarse-grained model for biomolecular phase separation with near-quantitative accuracy", Nature Computational Science **1**, 732–743 (2021).

[17]K. M. Ruff, T. S. Harmon, and R. V. Pappu, "Camelot: a machine learning approach for coarse-grained simulations of aggregation of block-copolymeric protein sequences", Journal of Chemical Physics **143**, 243123 (2015).

[18]G. L. Dignon, W. Zheng, and J. Mittal, *Simulation methods for liquid–liquid phase separation of disordered proteins*, Mar. 2019.

[19]J. M. Choi, F. Dar, and R. V. Pappu, "Lassi: a lattice model for simulating phase transitions of multivalent proteins", PLoS Computational Biology **15**, e1007028 (2019).

[20]P. J. Flory, "Thermodynamics of high polymer solutions", The Journal of Chemical Physics **10**, 51–61 (1942).

[21]M. T. Wei, S. Elbaum-Garfinkle, A. S. Holehouse, C. C. H. Chen, M. Feric, C. B. Arnold, R. D. Priestley, R. V. Pappu, and C. P. Brangwynne, "Phase behaviour of disordered proteins underlying low density and high permeability of liquid organelles", Nature Chemistry **9**, 1118–1125 (2017).

[22]T. J. Nott, E. Petsalaki, P. Farber, D. Jervis, E. Fussner, A. Plochowietz, T. D. Craggs, D. P. Bazett-Jones, T. Pawson, J. D. Forman-Kay, and A. J. Baldwin, "Phase transition of a disordered nuage protein generates environmentally responsive membraneless organelles", Molecular Cell **57**, 936–947 (2015).

[23]J. Berry, C. P. Brangwynne, and M. Haataja, *Physical principles of intracellular organization via active and passive phase transitions*, Feb. 2018.

[24]S. Mao, D. Kuldinow, M. P. Haataja, and A. Koš, "Phase behavior and morphology of multicomponent liquid mixtures †", 10.1039/c8sm02045k (2019).

[25]K. Shrinivas and M. P. Brenner, "Phase separation in fluids with many interacting components", Proceedings of the National Academy of Sciences **118**, e2108551118 (2021).

[26]W. M. Jacobs and D. Frenkel, *Phase transitions in biological systems with many components* (2017).

[27]A. D. Pezzutti and H. Hernández, "Unconditionally stable algorithm for copolymer and copolymer-solvent systems", Papers in Physics **12**, 120001 (2020).

[28]S. Alberti, A. Gladfelter, and T. Mittag, *Considerations and challenges in studying liquid-liquid phase separation and biomolecular condensates*, Jan. 2019.

[29]C. M. Fare, A. Villani, L. E. Drake, and J. Shorter, "Higher-order organization of biomolecular condensates", Open Biology **11**, 210137 (2021).

[30]J. W. Cahn and J. E. Hilliard, "Free energy of a nonuniform system. i. interfacial free energy", The Journal of Chemical Physics **28**, 258–267 (1958).

[31]M. Doi, *Soft matter physics* (Oxford University Press, June 2013).

[32]L. W. Chang, T. K. Lytle, M. Radhakrishna, J. J. Madinya, J. Vélez, C. E. Sing, and S. L. Perry, "Sequence and entropy-based control of complex coacervates", Nature Communications **8**, 10.1038/s41467-017-01249-1 (2017).

[33]B. A. Wolf, *Making floryr–huggins practical: thermodynamics of polymer-containing mixtures*, 2010.

[34]S. Puri, A. J. Bray, and J. L. Lebowitz, "Phase-separation kinetics in a model with order-parameter-dependent mobility", Phys. Rev. E **56**, 758–765 (1997).

[35]M. Muthukumar and S. Edwards, "Screening concepts in polymer solution dynamics", Polymer **23**, 345–348 (1982).

[36]P. M. Chaikin and T. C. Lubensky, *Principles of condensed matter physics* (Cambridge University Press, 1995).

[37]C. P. Guenther, "Pseudospectral techniques for non - smooth evolutionary problems", PhD thesis ().

[38]J. Zhu, L.-Q. Chen, J. Shen, and V. Tikare, "Coarsening kinetics from a variable-mobility cahn-hilliard equation: application of a semi-implicit fourier spectral method", Phys. Rev. E **60**, 3564–3572 (1999).

[39]P. Virtanen, R. Gommers, T. E. Oliphant, M. Haberland, T. Reddy, D. Cournapeau, E. Burovski, P. Peterson, W. Weckesser, J. Bright, S. J. van der Walt, M. Brett, J. Wilson, K. J. Millman, N. Mayorov, A. R. J. Nelson, E. Jones, R. Kern, E. Larson, C. J. Carey, İ. Polat, Y. Feng, E. W. Moore, J. VanderPlas, D. Laxalde, J. Perktold, R. Cimrman, I. Henriksen, E. A. Quintero, C. R. Harris, A. M. Archibald, A. H. Ribeiro, F. Pedregosa, P. van Mulbregt, and SciPy 1.0 Contributors, "SciPy 1.0: Fundamental Algorithms for Scientific Computing in Python", Nature Methods **17**, 261–272 (2020).

[40]J. W. Cooley and J. W. Tukey, "An algorithm for the machine calculation of complex fourier series", Mathematics of Computation **19**, 297–301 (1965).

[41]C. R. Harris, K. J. Millman, S. J. van der Walt, R. Gommers, P. Virtanen, D. Cournapeau, E. Wieser, J. Taylor, S. Berg, N. J. Smith, R. Kern, M. Picus, S. Hoyer, M. H. van Kerkwijk, M. Brett, A. Haldane, J. F. del Río, M. Wiebe, P. Peterson, P. Gérard-Marchant, K. Sheppard, T. Reddy, W. Weckesser, H. Abbasi, C. Gohlke, and T. E. Oliphant, "Array programming with NumPy", Nature **585**, 357–362 (2020).

[42]A. Bray, "Theory of phase-ordering kinetics", Advances in Physics **43**, 357–459 (1994).

[43]I. C. Henderson and N. Clarke, "Two-step phase separation in polymer blends", Macromolecules **37**, 1952–1959 (2004).

[44]N. Clarke, "Early stages of phase separation from polydisperse polymer mixtures", The European Physical Journal E **4**, 327–336 (2001).

[45]S. Puri, A. J. Bray, and J. L. Lebowitz, "Phase-separation kinetics in a model with order-parameter-dependent mobility", Physical Review E **56**, 758–765 (1997).

[46]D. Bonn and D. Ross, "Wetting transitions", Reports on Progress in Physics **64**, 1085–1163 (2001).

[47]K. Koga, J. O. Indekeu, and B. Widom, "Infinite-order transitions in density-functional models of wetting", Physical Review Letters **104**, 10.1103/physrevlett.104.036101 (2010).

[48]K. Koga and B. Widom, "Density functional models of the interfacial tensions near the critical endpoints and tricritical point of three-phase equilibria", Journal of Physics Condensed Matter **28**, 10.1088/0953-8984/28/24/244016 (2016).

Appendix A: Reflection

Comparing our final work to the project plan from the 22nd of October 2021 show a significant reduction of scope in comparison to what we finally decided to focus on in the second semester. This initial optimistic ambition meant that I spread myself out too thin, I explored many facets of this broad topic which would later become irrelevant once we began the project proper. I also tried to familiarize myself with theory and techniques which would prove useless when we finally decided on a research focus. In some sense I put the cart before the horse and should have taken a more measured and organized approach to the information acquisition section of the module, and properly contemplated what skills I require to carry out this project. This should involve scrutinizing the methodology of other work close to my chosen topic, by finding commonalities between methods I can come to conclusions on what is most appropriate to learn. In failing to internalize this lesson I was forced to play catch up at the later stages of this project which prevented me from fully investigating the phenomenon of interest and instead pivoting the dissertation to an assessment of my methods. My scatter shot approach is especially apparent in the literature review which was more of a superficial description of many different topics. This is not entirely my fault as the topics of liquid liquid phase separation and biomolecular condensates has generated a large body of research with many different subtopics. Parsing all this information in such a short time is very difficult, but I should have expressed more criticality when considering whether references are relevant. In this sense I have learnt many lessons from conducting this research, especially pertaining to the limits of my ability to assimilate large quantities of information.

There were some external problems which were beyond my control, one issue was concentration. Reading many papers and taking notes was a difficult task due to my learning difficulties, these were not treated at the time, and consequently I had great difficulty maintaining the concentration and will to write large reports and explore esoteric topics. Unfortunately, my supervisor had to go on leave for the last part of this project, this was not too much of a problem however, as Buddha's PHD student Biswaroop Mukherjee was a great guide on the material, and we were able to focus this dissertation to a simulation assessment, giving us a concrete target. Other issues arose form my mental health, as I've been experiencing family turmoil and a bereavement leading to some days where I would struggle to get the motivation to carry on with work. This unfortunately meant that some aspects of the project drew out longer than they should have, this again is especially the case with the literature review. Despite these facts, I feel quite accomplished in what I was able to accomplish. Regardless of this project's grade I have learnt many significant lessons, and feel more confident in my ability if I were to do this again.

Appendix B: Supplementary material

Minimisation of the free energy functional equation

The minimised functional $\frac{\mathcal{F}[\phi(r,t)]}{k_B T} = \int \left[f_b(\phi) + \kappa(\phi)(\nabla\phi)^2\right] d^d\vec{r}$ can be calculated from the Euler-Lagrange equation (*eq.*B1) for a constant κ giving us *eq.*B2.

$$\frac{\delta\mathcal{F}[\phi(\vec{r},t)]}{\delta\phi(\vec{r},t)} = \frac{\mathcal{F}[\phi(\vec{r},t)]}{\delta\phi} - \nabla\cdot\frac{\delta\mathcal{F}[\phi(\vec{r},t)]}{\delta\nabla\phi} \tag{B1}$$

$$\mu(\phi(\vec{r},t)) = \frac{\delta\mathcal{F}[\phi(\vec{r},t)]}{\delta\phi(\vec{r},t)} = \frac{\delta f_b}{\delta\phi} - 2\kappa\nabla^2\phi \tag{B2}$$

For non-constant κ we use calculus of variations (COV), starting with a small perturbation of the $\phi(\vec{r},t)$ profile by a minute quantity called ϵ at the vector $\vec{r}'$, where we consider $g(\vec{r},\vec{r}')$ to be a test function:

$$\frac{\delta\mathcal{F}[\phi(\vec{r},t)]}{\delta\phi(\vec{r},t)} = \lim_{\epsilon\to 0}\frac{1}{\epsilon}\left\{\mathcal{F}[\phi+\epsilon g(\vec{r},\vec{r}') - \mathcal{F}[\phi]]\right\} \tag{B3}$$

Applying COV to the the free energy and gradient term separately in our free energy functional results in an expression for the chemical potential:

$$\mu(\phi) = \frac{\delta\mathcal{F}}{\delta\phi} = \frac{\partial f_b}{\partial\phi} - (\nabla\phi)^2\frac{d\kappa(\phi)}{d\phi} - 2\kappa(\phi)\nabla^2\phi \tag{B4}$$

Substituting both derived chemical potentials into our Cahn-Hilliard equation. gives us an expression for both constant (*eq.*B5) and non constant (*eq.*B6) κ:

$$\frac{\delta\phi(\vec{r},t)}{\delta t} = \nabla\cdot\left[M(\phi)\nabla\left(\frac{\delta f_b}{\delta\phi} - 2\kappa\nabla^2\phi\right)\right] \tag{B5}$$

$$\begin{aligned}\frac{\partial\phi(\vec{r},t)}{\partial t} = {} & M(\phi)\nabla^2\left[\frac{\partial f_b}{\partial\phi} - (\nabla\phi)^2\frac{d\kappa(\phi)}{d\phi} - 2\kappa(\phi)\nabla^2\phi\right] \\ & + \nabla M(\phi)\cdot\nabla\left[\frac{\partial f_b}{\partial\phi} - (\nabla\phi)^2\frac{d\kappa(\phi)}{d\phi} - 2\kappa(\phi)\nabla^2\phi\right]\end{aligned}$$

Github link

All python code can be found in the following location: `https://github.com/BazzahN/pseudo-spectral-meth-of-CHE-`